NASA TN D-133

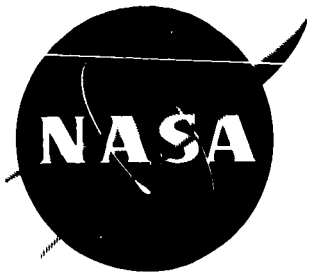

TECHNICAL NOTE

D-133

MEASUREMENTS OF HEAT TRANSFER AND FRICTION COEFFICIENTS FOR HELIUM FLOWING IN A TUBE AT SURFACE TEMPERATURES UP TO 5900° R

By Maynard F. Taylor and Thomas A. Kirchgessner

Lewis Research Center
Cleveland, Ohio

NATIONAL AERONAUTICS AND SPACE ADMINISTRATION

WASHINGTON October 1959

NATIONAL AERONAUTICS AND SPACE ADMINISTRATION

TECHNICAL NOTE D-133

MEASUREMENTS OF HEAT TRANSFER AND FRICTION COEFFICIENTS FOR HELIUM FLOWING IN A TUBE AT SURFACE TEMPERATURES UP TO 5900° R

By Maynard F. Taylor and Thomas A. Kirchgessner

SUMMARY

Measurements of average heat-transfer and friction coefficients and local heat-transfer coefficients were made with helium flowing through electrically heated smooth tubes with length-diameter ratios of 60 and 92 for the following range of conditions: average surface temperature from 1457° to 4533° R, Reynolds number from 3230 to 60,000, heat flux up to 345,000 Btu per hour per square foot of heat-transfer area, and exit Mach number to 1.0.

The results indicate that, in the turbulent range of Reynolds number based on tube diameter, good correlation of the local heat-transfer coefficients is obtained when the physical properties and density of helium are evaluated at a reference film temperature midway between the surface and fluid bulk temperatures. The average heat-transfer coefficients are best correlated on the basis that the coefficient varies with $[1 + (l/d)^{-0.7}]$ and the physical properties and density are evaluated at the surface temperature. The average friction coefficients for the tests with no heat addition are in complete agreement with the Kármán-Nikuradse line. The average friction coefficients for heat addition are in poor agreement with the accepted line.

INTRODUCTION

The importance of nuclear reactors as a power source for aircraft and space vehicles has stimulated interest in convective heat transfer from high-temperature surfaces. The resulting large ratio of fuel-element temperature to working-fluid temperature means a large variation in the properties of the fluid, which influence the heat-transfer characteristics. Some work has been done with wall temperatures up to 3460° R using air (ref. 1). Heat-transfer coefficients for helium flowing

through a carbon tube with a maximum inside surface temperature of 5040° R and a corresponding gas temperature of 4640° R are presented in reference 2.

In order to extend the range of surface temperature reported in reference 1 and the ratio of surface-to-fluid bulk temperature of reference 2, the experimental apparatus for the present investigation was set up at the NASA Lewis Research Center. In this investigation the wall temperatures were increased to the limit of the tungsten and molybdenum test sections, and the ratio of surface-to-fluid bulk temperature was kept as high as possible.

SYMBOLS

A	cross-sectional area of tube wall, ft
C_1	constant
C_2	constant, 25,891 micron-°R
c_p	specific heat of helium at constant pressure, Btu/(lb)(°R)
d	inside diameter of test section, ft
f	average friction coefficient
G	mass flow per unit cross-sectional area, lb/(hr)(sq ft)
g	acceleration due to gravity, 4.17×10^8 ft/hr^2
h	local heat-transfer coefficient, Btu/(hr)(sq ft)(°R)
h_{av}	average heat-transfer coefficient, Btu/(hr)(sq ft)(°R)
J_{bb}	rate of emission of radiant energy per unit wavelength interval at wavelength λ from unit area of black body, Btu/(hr)(sq ft)(micron)
J_{br}	rate of emission of radiant energy per unit wavelength interval at wavelength λ from unit area of non-black body, Btu/(hr)(sq ft)(micron)
J_τ	rate of transmission through view window of radiant energy per unit wavelength interval at wavelength λ from unit area of non-black body, Btu/(hr)(sq ft)(micron)

k	thermal conductivity of helium, Btu/(hr)(sq ft)($^{\circ}$R/ft)
k_t	thermal conductivity of test-section material, Btu/(hr)(sq ft)($^{\circ}$R/ft)
k_z	thermal conductivity of insulating material, Btu/(hr)(sq ft)($^{\circ}$R/ft)
l	heat-transfer length of test section, ft
Δl	incremental heat-transfer length, ft
Nu	Nusselt number based on local heat-transfer coefficient, hd/k
Nu_{av}	Nusselt number based on average heat-transfer coefficient, $h_{av}d/k$
P	absolute total pressure, lb/sq ft
Pr	Prandtl number, $c_p\mu/k$
Pr_f	$c_{p,f}\mu_f/k_f$
p	absolute static pressure, lb/sq ft
Δp	overall static-pressure drop across test section, lb/sq ft
Δp_{fr}	friction static-pressure drop across test section, lb/sq ft
Δp_{mom}	momentum static-pressure drop across test section, lb/sq ft
Q	rate of heat transfer to gas, Btu/hr
Q_c	rate of heat conduction through tube wall in axial direction, Btu/hr
Q_E	rate of electrical heat input to test section, Btu/hr
Q_e	rate of electrical heat input to increment, Btu/hr
Q_l	rate of heat loss to the surroundings, Btu/hr
$Q_{\Delta l}$	rate of heat loss radially to surroundings from an increment, Btu/hr
R	gas constant for helium, 386 ft-lb/(lb)($^{\circ}$R)
Re	Reynolds number, $\rho Vd/\mu$

Re_b	bulk Reynolds number, Gd/μ_b
Re_f	modified film Reynolds number, $\rho_f V d/\mu_f$
Re_s	modified surface Reynolds number, $\rho_s V d/\mu_s$
r_i	inside radius of insulating cylinder, ft
r_o	outside radius of insulating cylinder, ft
S	heat-transfer area of test section, sq ft
T	total or stagnation temperature, ^oR
T_b	average bulk temperature, $(T_1 + T_2)/2$, ^oR
T_{bb}	black-body temperature, ^oR
T_{br}	brightness temperature (apparent temp. of non-black body), ^oR
T_f	average film temperature, $(T_s + T_b)/2$, ^oR
T_s	average inside-surface temperature of test section, ^oR
$T_{z,i}$	temperature of inner wall of insulating cylinder, ^oR
$T_{z,o}$	temperature of outer wall of insulating cylinder, ^oR
T_τ	apparent brightness temperature (apparent temp. of non-black body with view window interposed), ^oR
t	static temperature, ^oR
V	bulk velocity of gas, ft/hr
w	helium flow, lb/hr
x	distance from entrance of test section, ft
γ	ratio of specific heats of helium
ε_λ	spectral emissivity
λ	wavelength (effective wavelength of small target optical-pyrometer filter), micron
μ	absolute viscosity of helium, lb/(hr)(ft)

ρ density of helium, lb/cu ft

ρ_{av} average density of helium defined by $(p_1 + p_2)/R(t_1 + t_2)$, lb/cu ft

τ_λ spectral transmissivity of view window

Subscripts:

b bulk (when applied to properties, indicates evaluation at av. bulk temp. T_b)

f film (when applied to properties, indicates evaluation at av. film temp. T_f)

s surface (when applied to properties, indicates evaluation at av. surface temp. T_s)

1 test-section entrance

2 test-section exit

EXPERIMENTAL APPARATUS

Arrangement

A schematic diagram of the arrangement of the test section and equipment used in the investigation is shown in figure 1. Dry helium, contained in a pressurized tank, was passed through the pressure-regulating valve into a rotameter and then to a mixing tank, which consisted of three concentric passages with baffles in the center passage. After mixing, the gas passed through the electrically heated test section into a second mixing tank of a design similar to the first tank and then exhausted into the atmosphere. The molybdenum test section was thermally insulated with a molybdenum radiation shield surrounded with zirconium oxide insulating grains. The zirconium oxide grains were held in place by a surrounding Transite cylinder. The tungsten test section was insulated only with a radiation shield. The mixing tanks, test section, and Transite cylinder were housed in a vacuum-tight steel containment tank, which was evacuated to about 50 microns of mercury. This was done to minimize oxidation of the refractory materials used as test sections. Pressures lower than 50 microns of mercury were possible but would have resulted in evaporation of the hot metals. Figure 2 shows a photograph of the setup with the containment tank removed.

Electric power was supplied to the test section through water-cooled copper tubing from a 208-volt 60-cycle supply line through a 100-kva power transformer and a 125-volt d-c saturable core reactor. The saturable core

reactor permitted voltage regulation from approximately 3 to 25 volts. A voltmeter was used directly to read the potential across the complete test section and across seven incremental lengths of the test section. Current was read on an ammeter used with an 800-to-1 current transformer.

Test Sections

Since the object of this investigation was to obtain heat-transfer data at as high a surface temperature as possible, this experiment embraced a number of materials problems. There are only five known metals with melting points above 5000° R: molybdenum, osmium, tantalum, rhenium, and tungsten, in order of increasing melting points. All five materials are subject to rapid oxidation when heated in air. For reasons of availability and high melting point, molybdenum and tungsten were chosen as test-section materials. Since molybdenum tubes were available commercially, they were used for the first tests. Several tubes were made by disintegrating holes through tungsten rods, which were then ground to a uniform wall thickness. Nickel entrance and molybdenum exit flanges were used to connect the test sections to the mixing tanks. A shrink fit combined with very careful welding was found to be a satisfactory method of attaching the flanges to the test section. The molybdenum test section was equipped with a bellmouth entrance. A right-angle edge approach was used for the tungsten test-section entrance.

The dimensions of the various tubes used as test sections in this investigation are as follows:

Tube material	Inside diam., d, in.	Outside diam., in.	Heat-transfer length, l, in.	l/d
Molybdenum	0.191	0.250	11.5	60
Tungsten	.125	.250	11.5	92

Instrumentation

The outside-wall temperatures of the test section were measured with 24-gage platinum - platinum-13-percent-rhodium thermocouples spot-welded along the length, located as shown in figure 3. For test-section temperatures beyond the range of the thermocouples, a small target optical pyrometer was used. The use of the optical pyrometer is discussed in the appendix. Some experimentation with tungsten-molybdenum thermocouples

was conducted, but the extreme brittleness of the tungsten wire after welding made the use of this thermocouple impractical.

The gas temperature was measured before entering and after leaving the test section with platinum - platinum-rhodium thermocouples located downstream of the baffles in the two mixing tanks.

The radiation shield and outside surface of the Transite insulating cylinder were instrumented with platinum - platinum-rhodium thermocouples. Molybdenum wire was spotwelded along the test section to measure voltage drop as a function of distance from the entrance. Locations are shown in figure 3. Static-pressure taps were located in the entrance mixing tank and in the entrance and exit flanges of the molybdenum test section, as shown in figure 3. The flanges of the tungsten test section were not instrumented with pressure taps because of the difficulty in getting holes through the walls of the tungsten tube.

TEST PROCEDURE

The following procedure was used in obtaining adiabatic friction data: The helium flow rate was set to a desired value; and, when steady-state conditions were attained, the flow rate, pressure readings, and inlet gas temperature were recorded. The helium flow rate was then set to a higher value; and, when steady-state conditions were attained, the experimental data were again recorded. The process was repeated until the available flow-rate range had been covered.

Heat-transfer and friction data for the heated test runs were obtained by the following general procedure: After the helium flow rate had been set to the desired value, the electric power across the test section was adjusted to give the desired test-section temperature. When steady-state conditions were attained, the flow rate, electrical power input, pressures, and temperatures were recorded. The helium flow rate and electrical power input were then set to higher values, and the process was repeated until the available Reynolds number range and test-section temperature range had been covered.

The molybdenum test section was used in obtaining both heat-transfer and friction-factor data. Since the tungsten test section was not instrumented with pressure taps, it was used only in obtaining heat-transfer data.

The range of conditions for which data were obtained is summarized in the following table:

Test-section material	Bulk Reynolds number, Re_b	Av. surface temp., T_s, $^\circ R$	Exit Mach number	Heat flux, Btu/(hr)(sq ft)
Molybdenum	3750 to 60,000	530	0.09 to 0.97	Adiabatic
Molybdenum	3230 to 25,230	1457 to 2334	0.21 to 0.95	71,000 to 290,000
Tungsten	5375 to 11,000	1905 to 4533	0.72 to 1.0	155,000 to 345,000

METHOD OF CALCULATION

Helium Properties

The variable physical properties of helium used in calculating the Nusselt, Reynolds, and Prandtl numbers are shown in figure 4 as a function of temperature. In the absence of experimental data, the curves in figure 4 were calculated by the methods shown in references 3 to 5. The value of specific heat c_p is 1.24 Btu/(lb)($^\circ$R) and is constant, the ratio of specific heats γ is 1.667, and the gas constant R is 386 ft-lb/(lb)($^\circ$R).

Friction Coefficients

Friction data were obtained both with and without heat transfer. The average friction coefficient was calculated from the experimental pressure-drop data as follows: The friction pressure drop Δp_{fr} was obtained by subtracting the calculated momentum pressure drop Δp_{mom} from the measured static-pressure drop, across the test section. Thus,

$$\Delta p_{fr} = \Delta p - \Delta p_{mom} = \Delta p - \frac{G^2 R}{g}\left(\frac{t_2}{p_2} - \frac{t_1}{p_1}\right) \qquad (1)$$

where t_1 and t_2 are the absolute static temperatures at the entrance and exit of the test section, respectively. In general, the static temperatures were calculated from the measured values of gas flow, static pressure, and the total temperature by the following equation, which is

obtained by combining the perfect gas law, the equation of continuity, and the energy equation:

$$t = -\frac{\gamma g}{(\gamma - 1)R}\left(\frac{p}{G}\right)^2 + \sqrt{\left[\frac{\gamma g}{(\gamma - 1)R}\left(\frac{p}{G}\right)^2\right]^2 + 2T\,\frac{\gamma g}{(\gamma - 1)R}\left(\frac{p}{G}\right)^2} \qquad (2)$$

For the bellmouth entrance, the static temperature t_1 could be represented by the relation

$$t_1 = T_1\left(\frac{p_1}{P_1}\right)^{\frac{\gamma-1}{\gamma}} \qquad (3)$$

In equation (3) the total pressure at the test-section entrance P_1 was assumed to be equal to the static pressure in the entrance mixing tank, where the velocity was negligible.

The average friction coefficient was calculated from the relation

$$f = \frac{\Delta p_{fr}}{4\frac{l}{d}\frac{\rho_{av}V^2}{2g}} = \frac{g\rho_{av}\Delta p_{fr}}{2\frac{l}{d}G^2} \qquad (4)$$

where the density ρ_{av} was evaluated at the average static pressure and temperature of the gas as follows:

$$\rho_{av} = \frac{1}{R}\left(\frac{p_1 + p_2}{t_1 + t_2}\right) \qquad (5)$$

The average friction coefficient was also calculated with the density evaluated at the film temperature, as shown in the following equation:

$$f_f = \frac{\Delta p_{fr}}{4\frac{l}{d}\frac{\rho_f V^2}{2g}} = \left(\frac{\rho_{av}}{\rho_f}\right)f = \left(\frac{2T_f}{t_1 + t_2}\right)f \qquad (6)$$

Heat-Transfer Coefficient

The average heat-transfer coefficient h_{av} was computed from the experimental data by the relation

$$h_{av} = \frac{Q}{S(T_s - T_b)} \qquad (7)$$

where

$$Q = wc_{p,b}(T_2 - T_1) \tag{8}$$

and the average surface temperature T_s was taken as an integrated average of the local outside wall temperature minus the temperature drop through the wall. The temperature of the gas T_b was taken as the arithmetic mean of the total temperatures at the entrance T_1 and the exit T_2 of the test section.

The average heat-transfer coefficient was used to calculate the Nusselt number from the following relation:

$$Nu_{av} = \frac{h_{av}d}{k} \tag{9}$$

The Nusselt number was calculated with thermal conductivities evaluated at surface, bulk, and film temperatures.

The heat loss to the surroundings was calculated by the following equation:

$$Q_l = Q_E - Q \tag{10}$$

For most runs, more than 80 percent of the heat generated was transferred to the gas.

It was possible to calculate local heat-transfer coefficients by evaluating the various local heat losses and then making a heat balance. The heat losses were calculated as follows:

(1) The heat loss at the ends of the test section by conduction was calculated from the following equation:

$$Q_c = k_t A \frac{dT}{dl} \tag{11}$$

where dT/dl is the slope of the axial wall temperature distribution at the entrance and exit of the test section.

(2) Local radial heat loss through the insulation for each increment of length Δl was calculated with the following equation:

$$Q_{\Delta l} = k_z \frac{2\pi\Delta l}{\ln \frac{r_o}{r_i}} (T_{z,i} - T_{z,o}) \tag{12}$$

where k_z is the thermal conductivity of the insulation evaluated at the average insulation temperature.

(3) The sum of the local radial heat losses and the end losses was found to account for more than 80 percent of the total heat loss calculated by equation (10). Each local heat loss and the end losses were increased by the ratio of total heat loss to the sum of local heat losses.

(4) The rate of heat conduction into and away from each increment, $Q_{c,in}$ and $Q_{c,out}$, respectively, was calculated using equation (11) and taking dT/dl as the slope of the axial temperature distribution at the ends of the increment being calculated.

(5) The rate of electrical heat generation in each increment Q_e was calculated by multiplying the current through the test section by the voltage drop across the increment.

(6) A heat balance was then set up for each increment starting at the entrance, as follows:

$$Q_e + Q_{c,in} - Q_{c,out} - Q_{\Delta l} - Q = 0 \qquad (13)$$

from which it was possible to calculate the rate of heat transfer to the gas Q from each increment. The bulk temperature of the gas leaving each increment could be calculated by using the equation

$$Q = wc_{p,b} (T_{out} - T_{in}) \qquad (14)$$

where T_{in} is the bulk temperature of the gas entering the increment, and T_{out} is the bulk temperature of the gas leaving the increment. This was repeated for each succeeding increment, and the outlet gas temperature was compared with the measured outlet gas temperature (station 2) as a check on the computation.

(7) The local bulk temperature and local surface temperature along with the heat-transfer area for the increment and the rate of heat transfer to the gas for the increment were used to calculate a local heat-transfer coefficient using the same type of equation used to calculate the average heat-transfer coefficient. Nusselt number based on the local heat-transfer coefficient was calculated and will be discussed along with the average Nusselt number in the following section.

RESULTS AND DISCUSSION

Axial Wall Temperature Distributions

In figure 5 representative axial outside-wall temperatures are shown for a tungsten tube with a length-diameter ratio of 92. The outside-wall

temperature is plotted against dimensionless distance x/l for three different average inside-wall temperatures T_s. The rate of heat transfer to the gas Q, the mass flow w, the ratio of average surface to bulk temperature T_s/T_b, the temperature rise of the gas $T_2 - T_1$, and the thermocouple and optical-pyrometer temperature measurements are given in figure 5.

The increase in the slope of each axial wall temperature distribution is probably due to the increase in resistivity with temperature (the resistivity at 4000° R is twice that at 2000° R). The large axial temperature gradients at the entrance and exit of the test section are the result of conduction losses to the connecting flanges, mixing tanks, and electrical connectors.

Friction Coefficients

The average friction coefficients for both the adiabatic and heated runs are shown in figure 6. The line representing the Kármán-Nikuradse relation between friction coefficient and Reynolds number for turbulent flow

$$\frac{1}{\sqrt{\frac{8f}{2}}} = 2 \log \left(\mathrm{Re} \sqrt{\frac{8f}{2}} \right) - 0.8 \tag{15}$$

and the laminar-flow line

$$\frac{f}{2} = \frac{8}{\mathrm{Re}} \tag{16}$$

are included in figure 6 for comparison.

For Reynolds numbers above 6000, the average friction coefficients for adiabatic flow are in very good agreement with the turbulent-flow line. In the lower Reynolds number region the coefficients drop off and approach the laminar-flow line, as would be expected in the transition region. The extension of the transition region to a Reynolds number of 6000 was due to the effect of the bellmouth entrance. The average friction coefficients with the density evaluated at bulk temperature (eq. (5)) are shown in figure 6(a). The data from the present investigation are in fair agreement with the predicted line for the higher Reynolds number range.

References 1 and 6 indicate that average friction coefficients are best correlated with density evaluated at the film temperature and with a modified Reynolds number based on film temperature. Data from the

present investigation and reference 6 are shown evaluated in this manner in figure 6(b). The friction coefficients are somewhat higher than the Kármán-Nikuradse line, but good agreement exists with the data of reference 6.

Heat-Transfer Coefficients

The results of reference 1 indicate that the average Nusselt number for various ratios of surface-to-bulk temperature and length to diameter is best represented by the following:

$$(Nu_{av})_f = \frac{h_{av}d}{k_f} = 0.034\ Re_f^{0.8} Pr_f^{0.4} \left(\frac{l}{d}\right)^{-0.1} \tag{17}$$

where all the physical properties and the density are evaluated at the film temperature, and the modified Reynolds number is used.

An alternative method of correcting for the effect of the length-to-diameter ratio is the use of the following equation:

$$(Nu_{av})_f = \frac{h_{av}d}{k_f} = 0.021\ Re_f^{0.8} Pr_f^{0.4} \left[1 + \left(\frac{l}{d}\right)^{-0.7}\right] \tag{18}$$

where the use of $[1 + (l/d)^{-0.7}]$ in place of $(l/d)^{-0.1}$, and the corresponding difference in constants, makes the relation more general, since it is applicable to all length-diameter ratios. The data of the present investigation with the properties evaluated at the film temperature are shown in figure 7(a) as a function of modified Reynolds number. For Reynolds numbers less than 10,000 the present data are in poor agreement with equation (18). Above a Reynolds number of 10,000 the data agree to within 10 percent.

For the limited range of Reynolds number in this investigation, the average heat-transfer data seem to be correlated better by evaluating the physical properties and density at the surface temperature. The results are shown in figure 7(b). Experimental data from reference 1 using air and a platinum test section at average tube surface temperatures from 980° to 3050° R are shown in both figures 7(a) and (b).

Since there could be some question as to the significance of average heat-transfer coefficients when the heat flux varies as much as is indicated by the axial wall temperature distributions shown in figure 5, it seemed desirable to calculate local heat-transfer coefficients. Ratios of local surface temperature to local bulk temperatures were considerably higher than ratios of the averages of these temperatures. Local heat-transfer data are shown in figure 8(a), where the film Nusselt number is

plotted as a function of modified Reynolds number. The data are in fair agreement with the line represented by the following equation:

$$Nu_f = \frac{hd}{k_f} = 0.021\ Re_f^{0.8} Pr_f^{0.4} \qquad (19)$$

The same data, shown in figure 8(b) with the physical properties and desnity evaluated at the surface temperature T_s, fall higher than the predicted line. However, the spread of the data is decreased from about 38 percent in figure 8(a) to about 25 percent in figure 8(b). Heat-transfer coefficients for the first two increments and the last increment were not used because of entrance effects and the large end losses.

SUMMARY OF RESULTS

The following summary gives the results of this investigation of heat transfer and pressure drop for helium flowing through electrically heated smooth tubes with length-diameter ratios of 60 and 92 for the following range of conditions: average surface temperature from 1457° to 4533° R, Reynolds number from 3230 to 60,000, heat flux up to 345,000 Btu per hour per square foot of heat-transfer area, and exit Mach number to 1.0:

1. In general, the correlation of both local and average heat-transfer coefficients is in agreement with that of previous investigations of average heat-transfer coefficients at lower surface temperatures and heat flux. The physical properties and density used in the Nusselt, Prandtl, and Reynolds numbers were evaluated at the film temperature, which is midway between the surface and bulk temperatures; a modified Reynolds number was used; and a correction for length-diameter ratio was applied to the average Nusselt number. For low Reynolds numbers, better correlation of the average Nusselt number results if the physical properties and density are evaluated at the surface temperature.

2. Friction coefficients with no heat transfer are in good agreement with those obtained by other investigators. The friction coefficients obtained with heat addition are in fair agreement with the Kármán-Nikuradse line when the average density is evaluated at the gas temperature. Evaluation of the density at the film temperature, as done in previous investigations, gave rather poor agreement with the accepted line.

Lewis Research Center
National Aeronautics and Space Administration
Cleveland, Ohio, August 4, 1959

APPENDIX - METHOD OF OPTICAL PYROMETRY

As mentioned in the text, the temperatures above approximately 3500° R were measured with an optical pyrometer. Since the insulated test section did not approximate a black body, it was necessary to correct the temperature readings of the pyrometer.

A relation between the true temperature of an object and the brightness temperature indicated by the optical pyrometer can be obtained from Wien's formula for black-body radiation

$$J_{bb} = C_1 \lambda^{-5} e^{-C_2/\lambda T_{bb}} \tag{A1}$$

where J_{bb} is the rate of emission of radiant energy at wavelength λ from a black body at temperature T_{bb}, and C_1 and C_2 are known constants. The same formula can be applied to a non-black body at true temperature T_{bb}, and can be written

$$J_{br} = \varepsilon_\lambda C_1 \lambda^{-5} e^{-C_2/\lambda T_{bb}} = C_1 \lambda^{-5} e^{-C_2/\lambda T_{br}} \tag{A2}$$

where T_{br} is the brightness temperature.

The ratio of J_{br} to J_{bb} is defined as the spectral emissivity ε_λ of the non-black body under consideration, as follows:

$$\varepsilon_\lambda = \frac{J_{br}}{J_{bb}} = \frac{C_1 \lambda^{-5} e^{-C_2/\lambda T_{br}}}{C_1 \lambda^{-5} e^{-C_2/\lambda T_{bb}}} \tag{A3}$$

Therefore,

$$\ln \varepsilon_\lambda = -\frac{C_2}{\lambda T_{br}} + \frac{C_2}{\lambda T_{bb}} = \frac{C_2}{\lambda}\left(\frac{1}{T_{bb}} - \frac{1}{T_{br}}\right) \tag{A4}$$

The interposition of a view window between the heated object and the optical pyrometer necessitates a modification of equation (A4) to include the spectral transmissivity τ_λ of the window. The spectral transmissivity is defined as the ratio of the transmitted radiant energy to the incident radiant energy for a given wavelength:

$$\tau_\lambda = \frac{J_\tau}{J_{br}} = \frac{C_1 \lambda^{-5} e^{-C_2/\lambda T_\tau}}{C_1 \lambda^{-5} e^{-C_2/\lambda T_{br}}} \tag{A5}$$

where T_τ is the temperature of a heated body measured with the optical pyrometer with the window interposed, and T_{br} is the optical-pyrometer

brightness temperature measured under the same conditions with the exception that no window is interposed. Both measurements would be made while the black-body temperature remained constant. Equation (A5) can also be expressed as

$$\ln \tau_\lambda = \frac{C_2}{\lambda}\left(\frac{1}{T_{br}} - \frac{1}{T_\tau}\right) \tag{A6}$$

Solving equation (A6) for T_{br} gives

$$T_{br} = \frac{C_2/\lambda}{\ln \tau_\lambda + \frac{C_2}{\lambda T_\tau}} \tag{A7}$$

and substituting this expression for T_{br} into equation (A4) gives

$$\ln(\varepsilon_\lambda \tau_\lambda) = \frac{C_2}{\lambda}\left(\frac{1}{T_{bb}} - \frac{1}{T_\tau}\right) \tag{A8}$$

which can be written

$$T_{bb} = \frac{C_2/\lambda}{\ln(\varepsilon_\lambda \tau_\lambda) + \frac{C_2}{\lambda T_\tau}} \tag{A9}$$

This expression can be used to calculate the actual temperature of a heated body if the spectral emissivity of the heated body ε_λ and the transmissivity of the window τ_λ are known, and the temperature T_τ is measured with an optical pyrometer.

The transmissivity of a view window can be determined very easily experimentally by measuring the temperature of a calibration lamp both with and without the window interposed and by inserting these values into equation (A6).

There are values of spectral emissivity for tungsten and molybdenum in the literature, but these values are for flat polished specimens with all radiation originating from the specimen. These conditions are not very closely approximated by most heat-transfer test sections; for example, the test sections used in the present investigation were circular tubes whose surfaces did not remain polished because of grain growth and a small amount of oxidation; some of the radiation incident to the optical pyrometer was emitted and reflected from the hot radiation shield. As a matter of fact, it is more correct to say that it is the effective spectral emissivity that is of interest. The method of determining this effective emissivity was to measure the temperature of the test section with an optical pyrometer and thermocouple simultaneously, and then insert the values into equation (A8) to obtain a value for $\ln(\varepsilon_\lambda \tau_\lambda)$. This

value could be used to compute ϵ_λ, since τ_λ had been previously determined. The values of ϵ_λ could be plotted as a function of temperature up to the point where the thermocouples failed (about 3500° R) and then extrapolated to the higher temperatures. With these values of ϵ_λ and τ_λ, equation (A9) could be used to determine the true wall temperature with the optical pyrometer.

The values for effective spectral emissivity might have been in error, especially in the extrapolated region. The effect of an error in emissivity on the test-section wall temperature calculated by equation (A9) is tabulated as follows:

Measured temperature, T_τ, °R	Effective spectral emissivity, $\epsilon_\lambda \tau_\lambda$	Calculated true temperature, T_{bb}, °R
5460	0.5	6030
5460	.6	5870
5460	.7	5740

From this table it can be seen that fairly large errors in effective spectral emissivity do not seem to affect the wall temperature appreciably.

REFERENCES

1. Humble, Leroy W., Lowdermilk, Warren H., and Desmon, Leland G.: Measurements of Average Heat-Transfer and Friction Coefficients for Subsonic Flow of Air in Smooth Tubes at High Surface and Fluid Temperatures. NACA Rep. 1020, 1951. (Supersedes NACA RM's E7L31, E8L03, E50E23, and E50H23.)

2. Durham, F. P., Neal, R. C., and Newman, H. J.: High Temperature Heat Transfer to a Gas Flowing in Heat Generating Tubes with High Heat Flux. TID-7529, pt. 1, book 2, Reactor Heat Transfer Conf., Nov. 1957. pp. 502-514.

3. Woolley, Harold W.: Helium. Table 6.10 of the NBS-NACA Tables of Thermal Properties of Gases, NBS, 1950.

4. Nuttall, R. L.: Helium. Table 6.39 of the NBS-NACA Tables of Thermal Properties of Gases, NBS, 1950.

5. Nuttall, R. L.: Helium. Table 6.42 of the NBS-NACA Tables of Thermal Properties of Gases, NBS, 1950.

6. Weiland, Walter F., and Lowdermilk, Warren H.: Measurements of Heat-Transfer and Friction Coefficients for Air Flowing in a Tube of Length-Diameter Ratio of 15 at High Surface Temperatures. NACA RM E53E04, 1953.

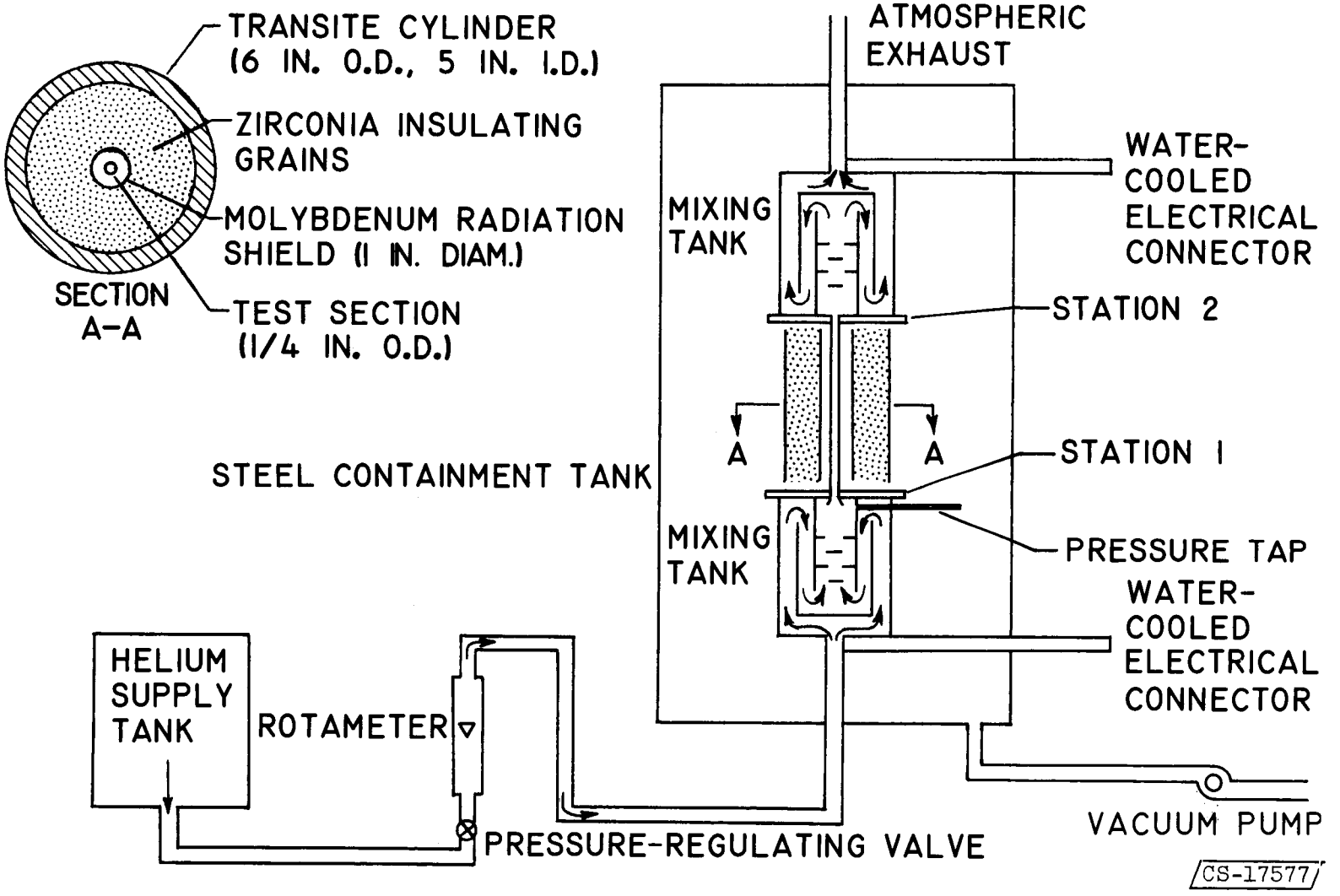

Figure 1. - Schematic diagram showing arrangement of test apparatus.

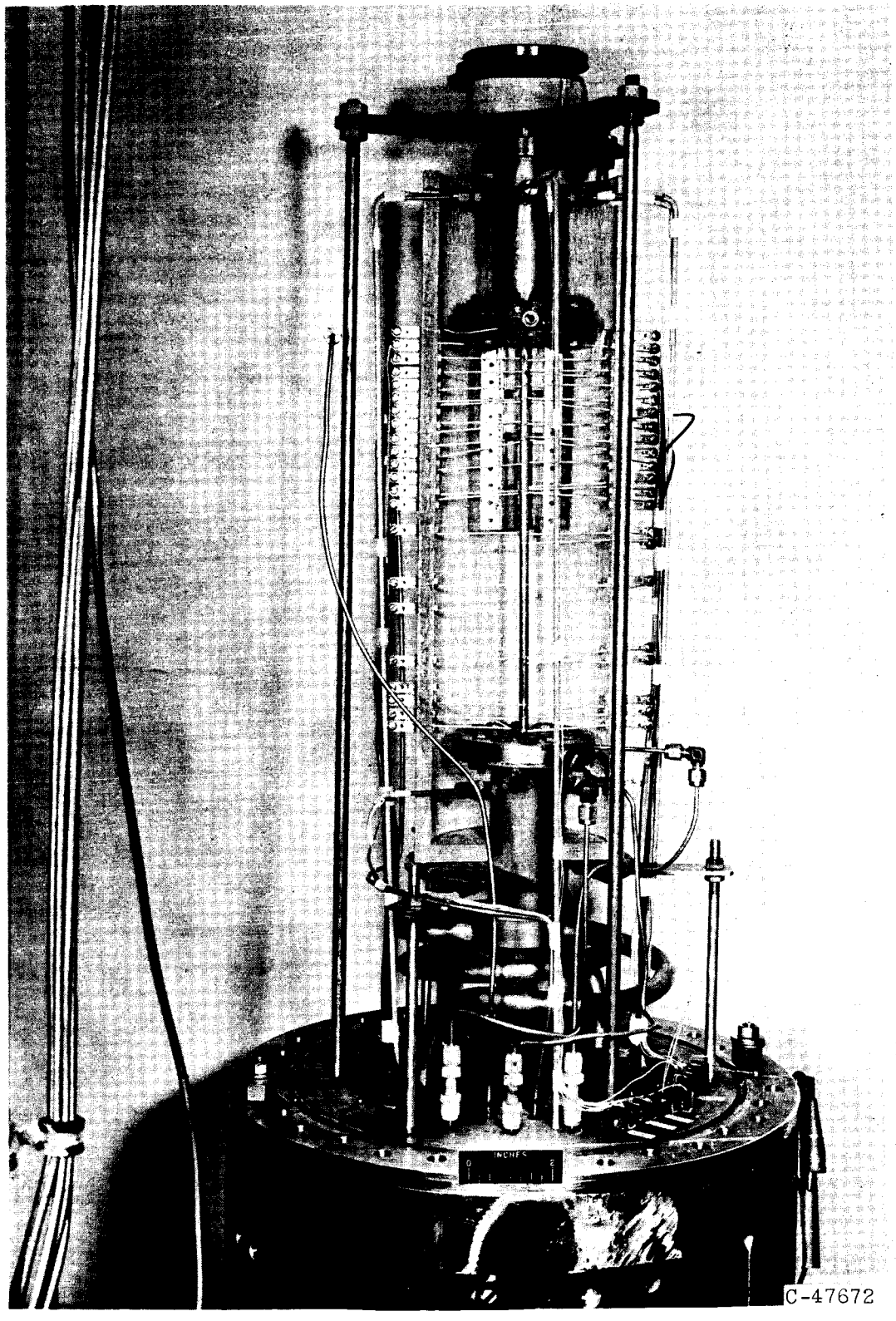

Figure 2. - High-temperature heat-transfer apparatus.

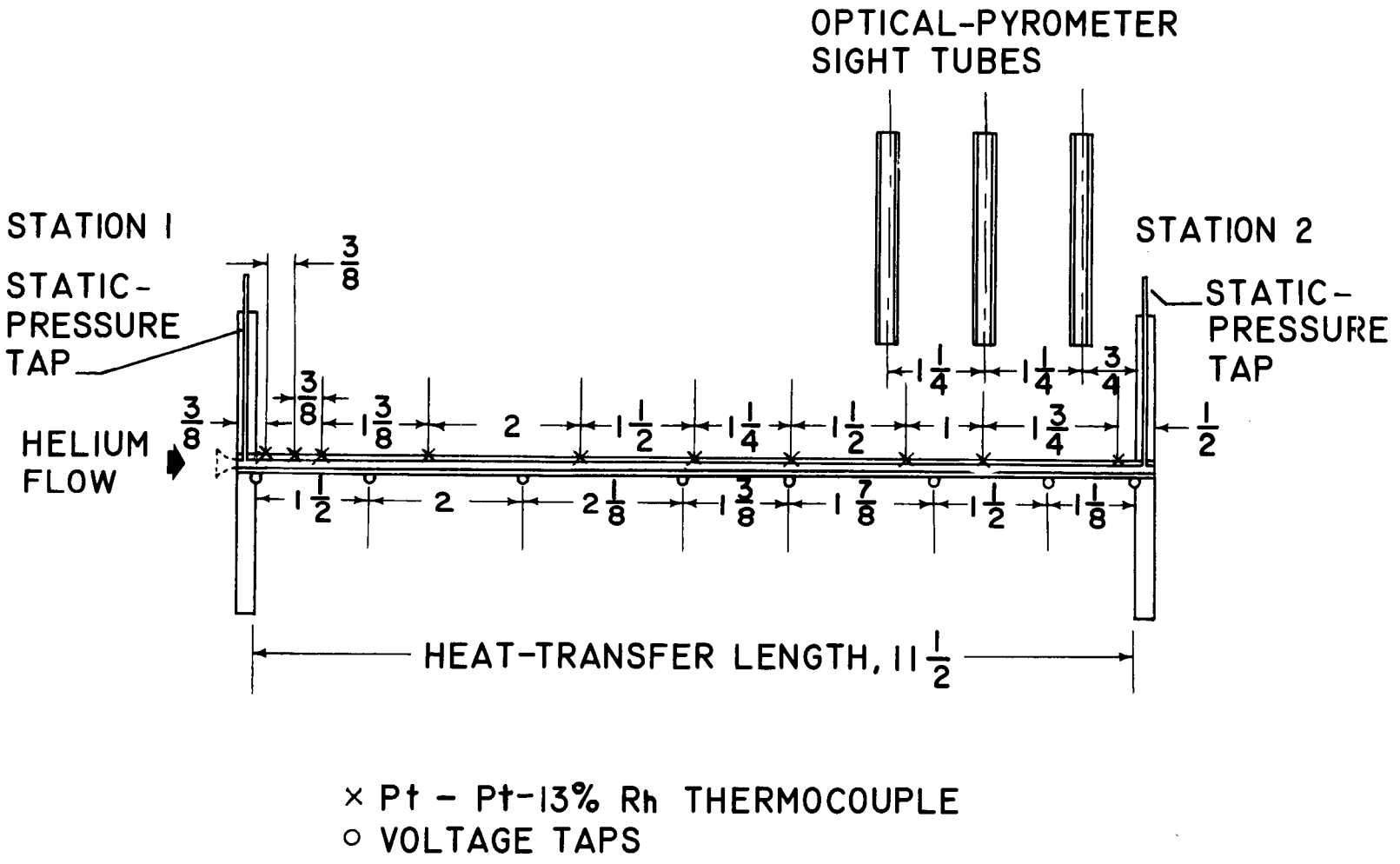

Figure 3. - Typical test section. Thermocouple, optical pyrometer, voltage tap, and pressure tap locations shown are for molybdenum test section. (All dimensions in inches.)

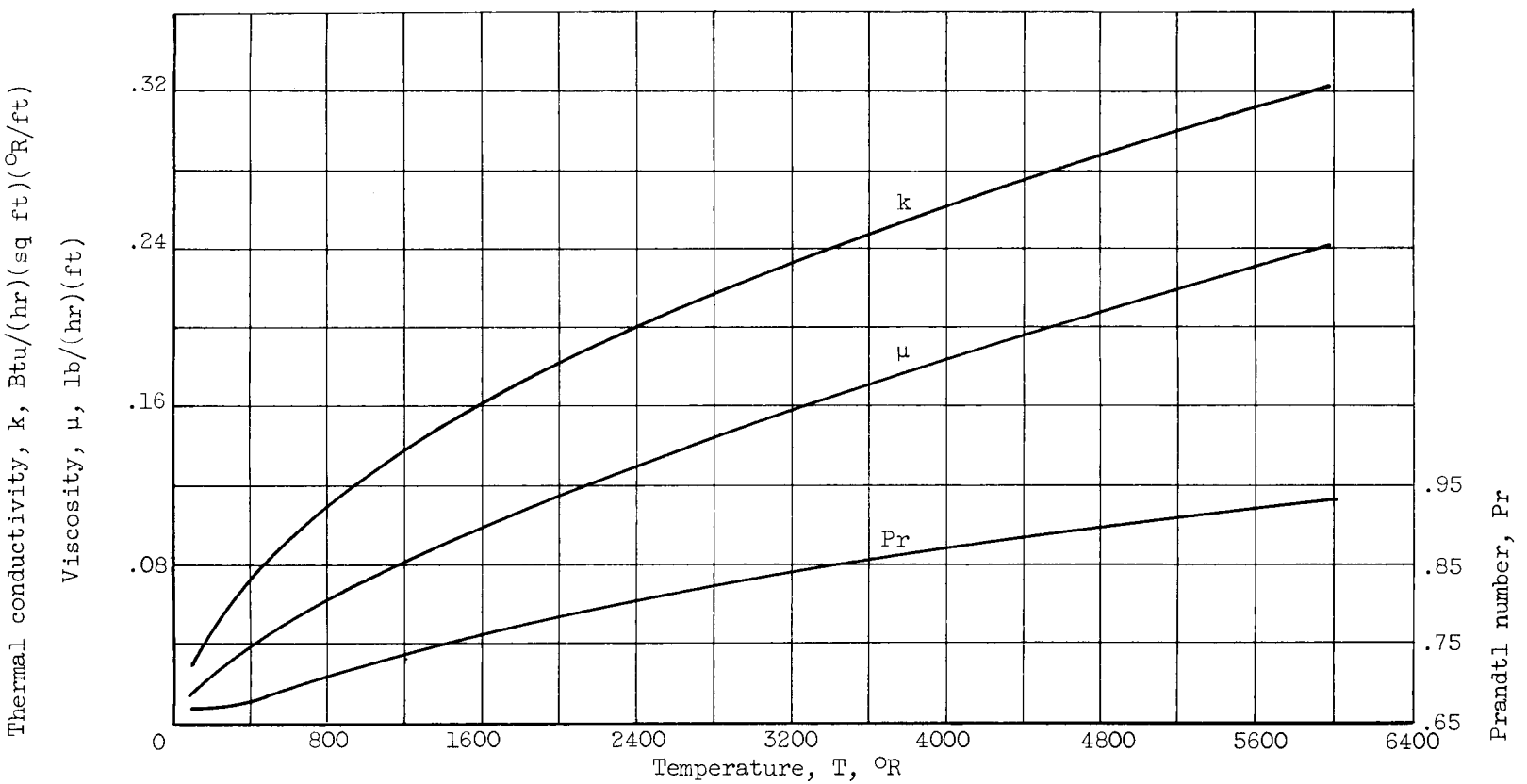

Figure 4. - Variation of thermal conductivity, absolute viscosity, and Prandtl number of helium with temperature.

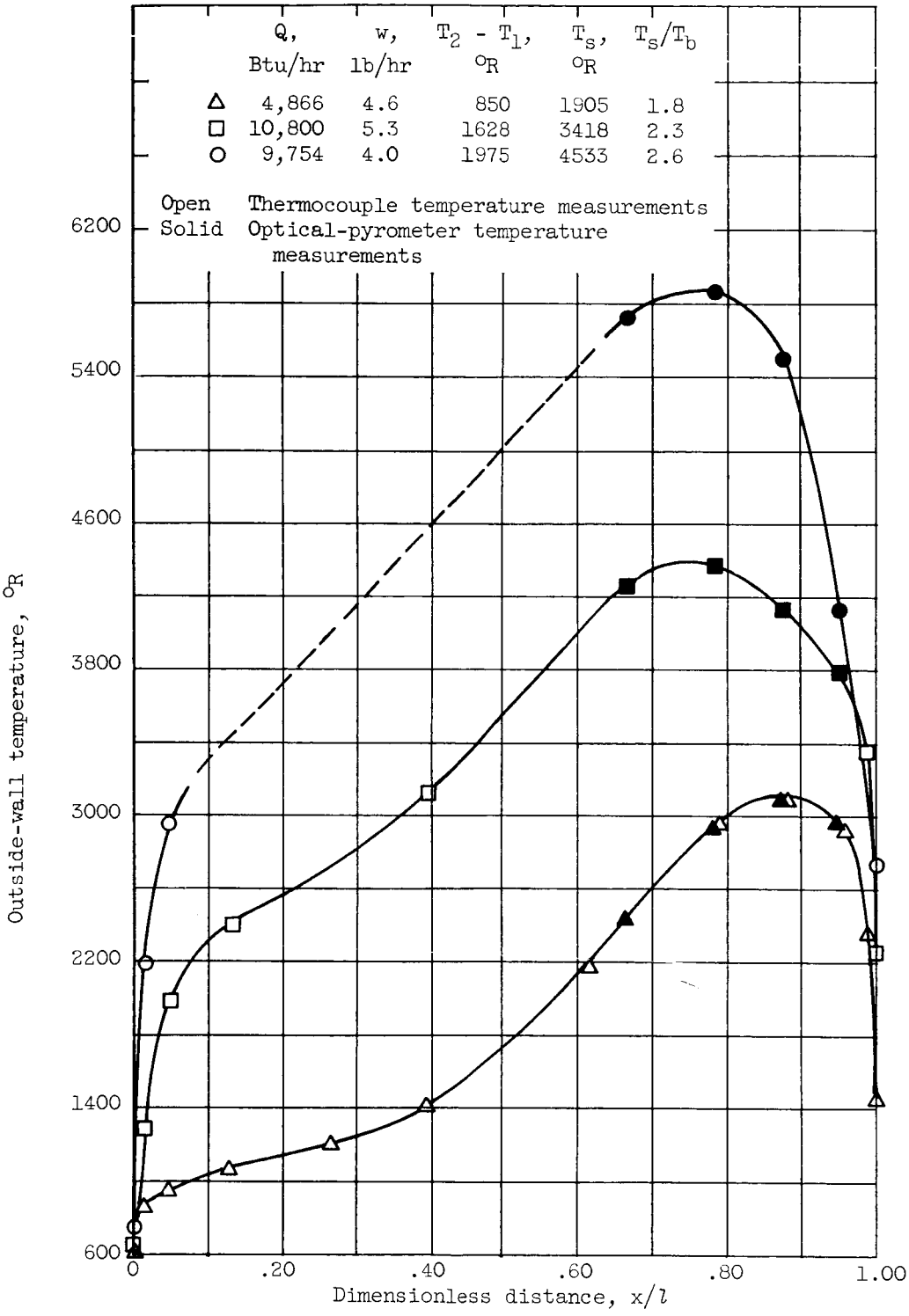

Figure 5. - Representative outside-wall temperature distribution for various amounts of heat input to helium. Tungsten tube; length-diameter ratio, 92.

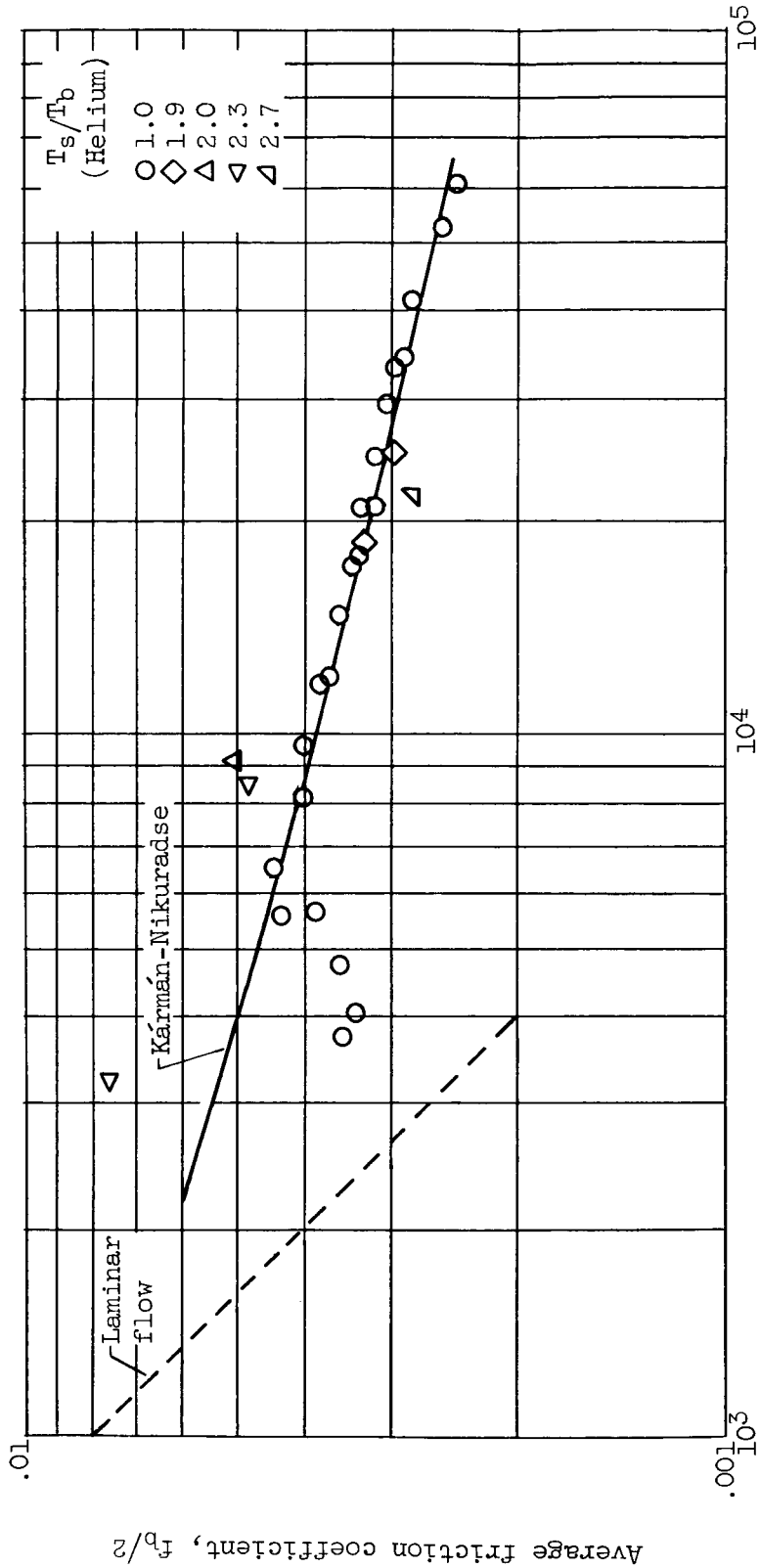

(a) Viscosity and density evaluated at bulk temperature T_b. Kármán-Nikuradse relation, $1/\sqrt{8f_b/2} = 2 \log(Re_b\sqrt{8f_b/2}) - 0.8$; laminar flow, $f_b/2 = 8/Re_b$.

Figure 6. - Correlation of average friction coefficients.

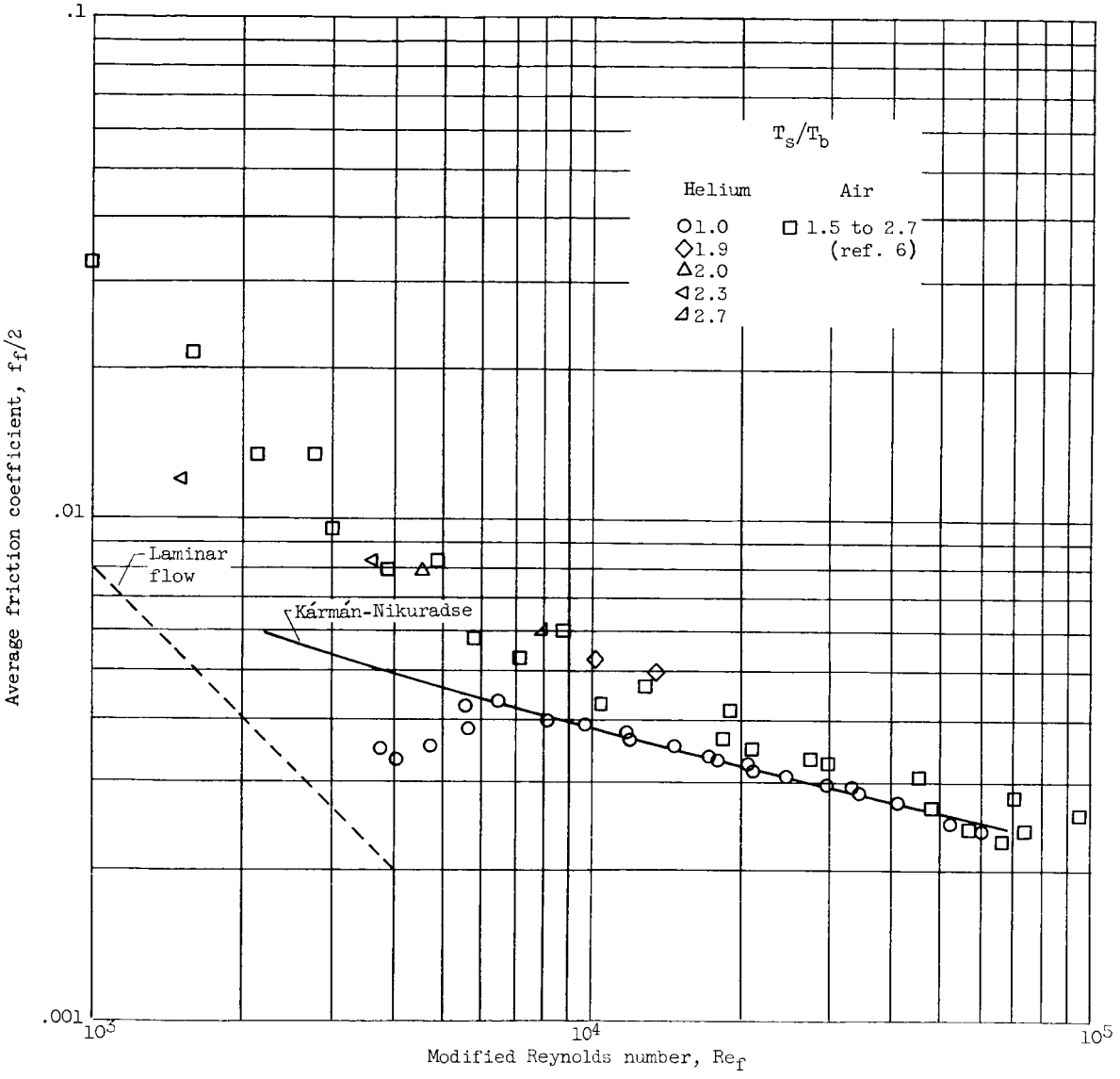

(b) Viscosity and density evaluated at film temperature T_f. Kármán-Nikuradse relation, $1/\sqrt{8f_f/2} = 2 \log(Re_f\sqrt{8f_f/2}) - 0.8$; laminar flow, $f_f/2 = 8/Re_f$.

Figure 6. - Concluded. Correlation of average friction coefficients.

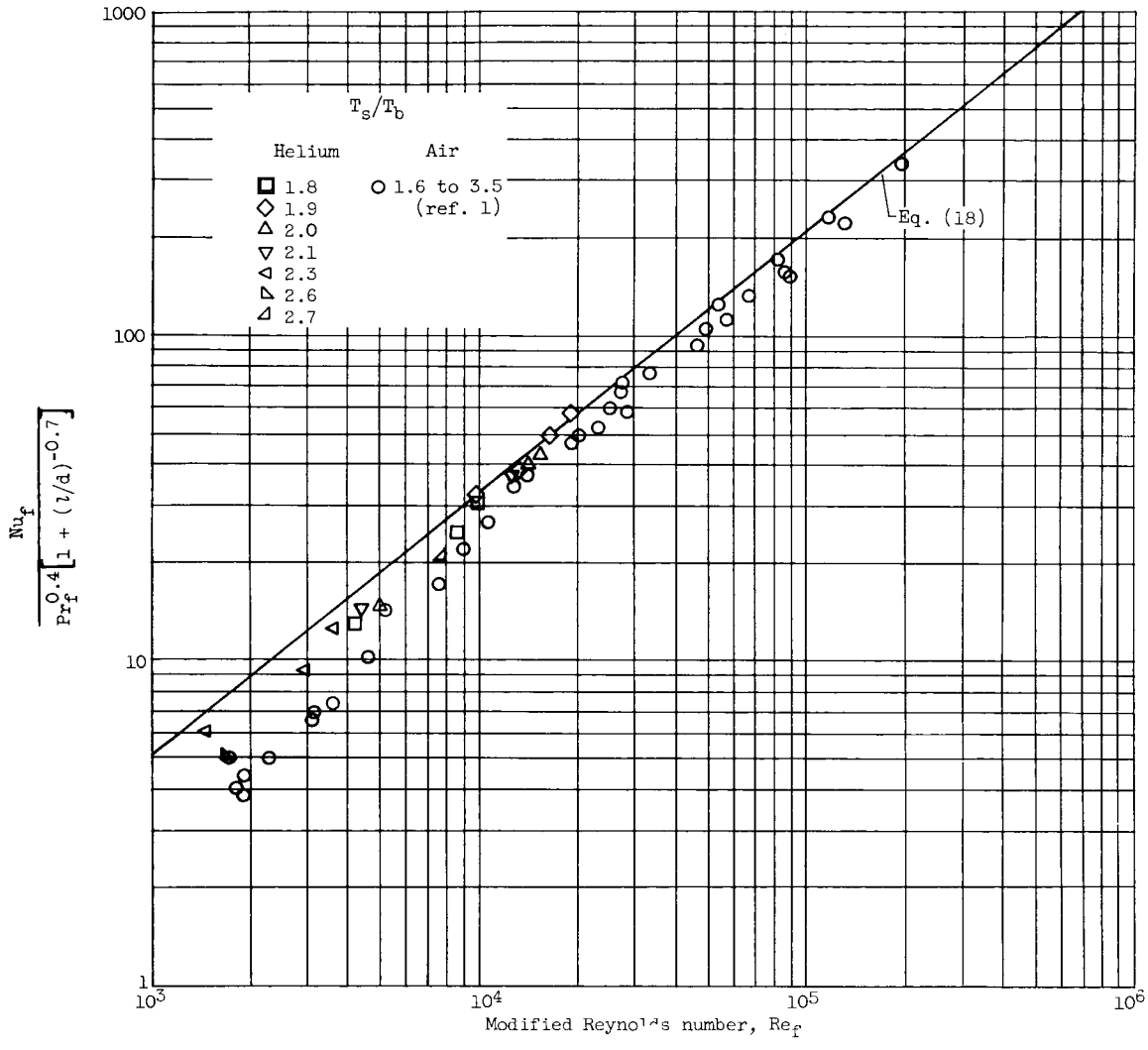

(a) Properties of helium evaluated at film temperature T_f.

Figure 7. - Correlation of average heat-transfer coefficients with variable heat flux. Length-diameter ratios, 60 and 92.

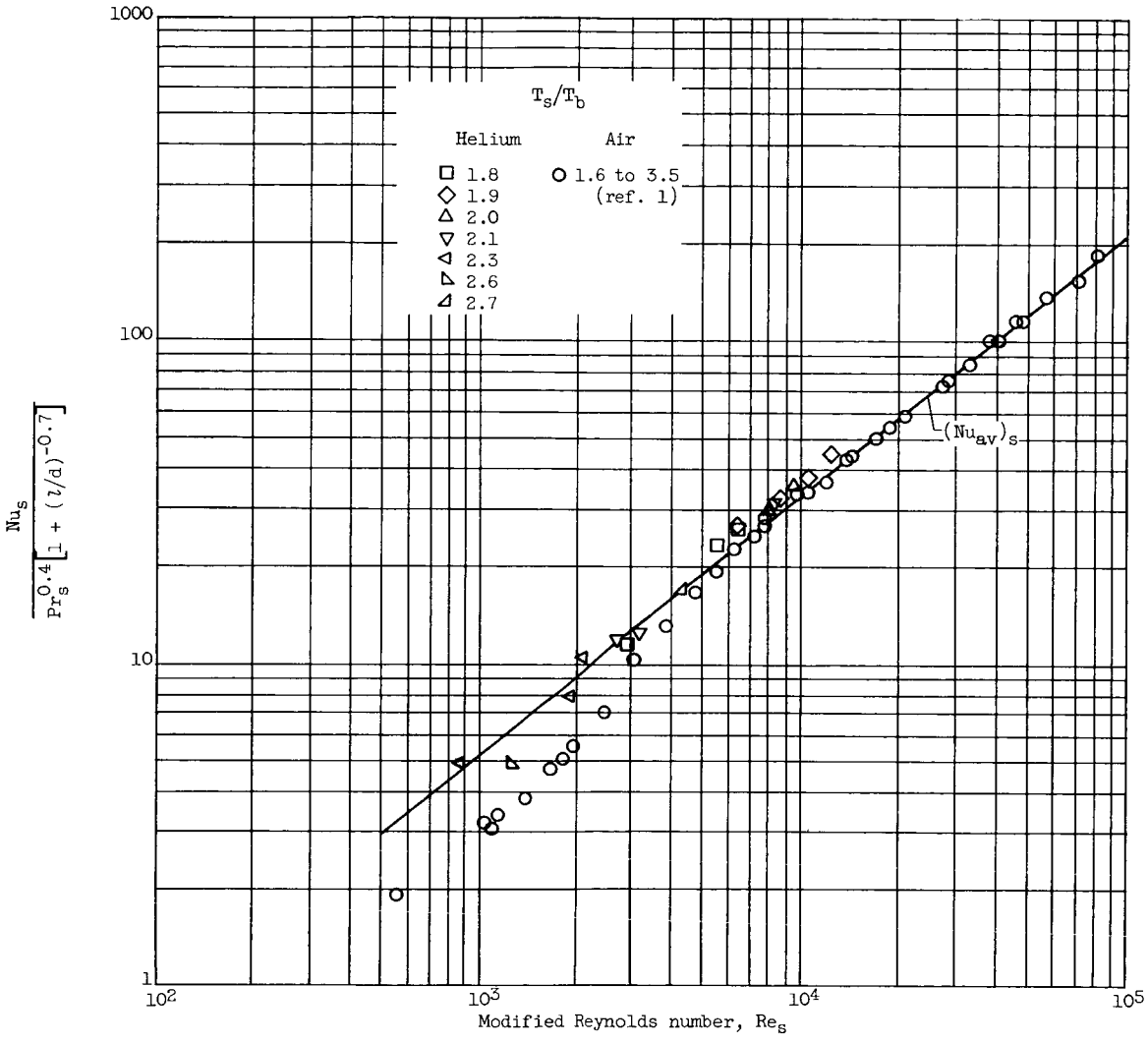

(b) Properties of helium evaluated at surface temperature T_s.

Average Nusselt number $(Nu_{av})_s = \frac{h_{av}d}{k_s} = 0.021\ Re_s^{0.8} Pr_s^{0.4}\left[1 + \left(\frac{l}{d}\right)^{-0.7}\right]$.

Figure 7. - Concluded. Correlation of average heat-transfer coefficients with variable heat flux. Length-diameter ratios, 60 and 92.

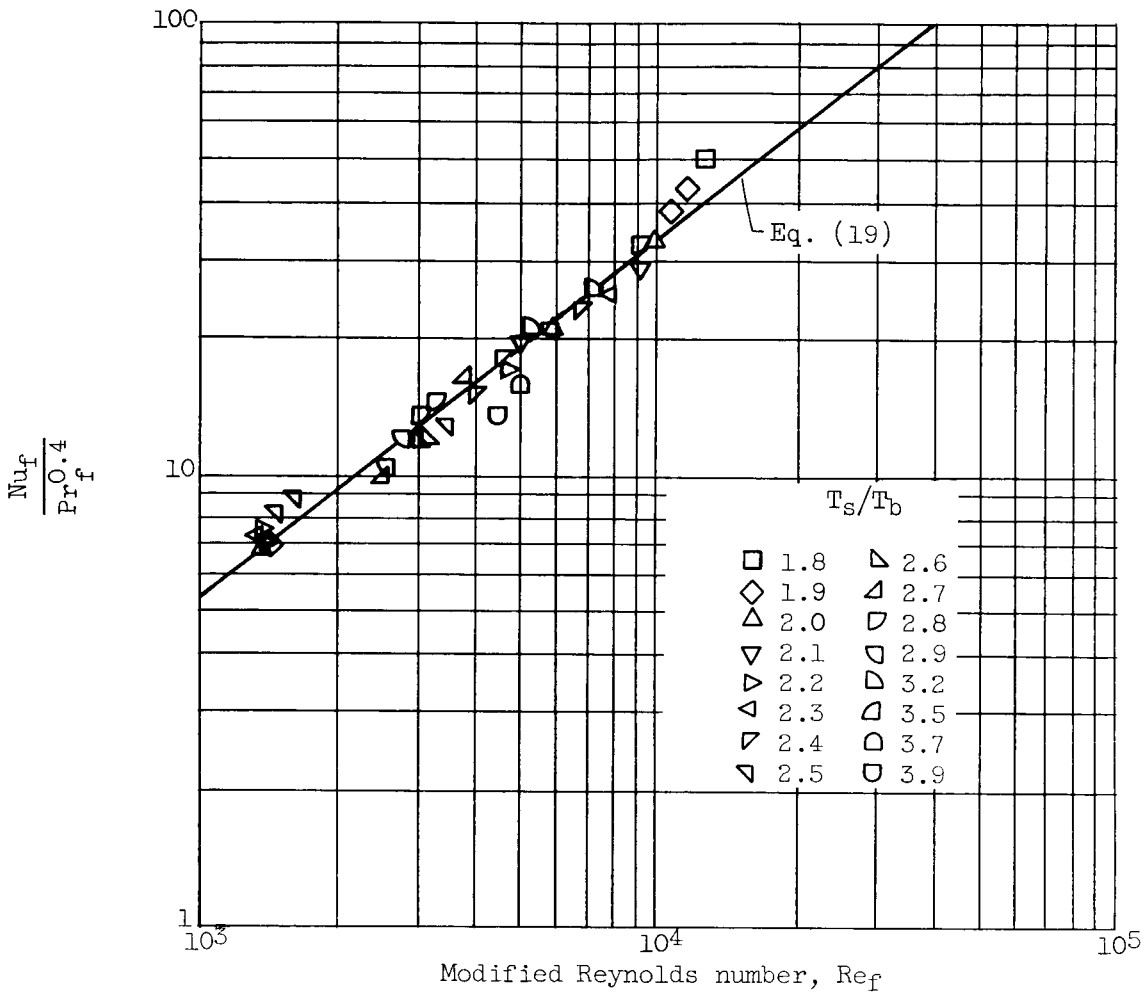

(a) Properties of helium evaluated at film temperature T_f.

Figure 8. - Correlation of local heat-transfer coefficients with variable heat flux. Overall length-diameter ratio, 60; bellmouth entrance.

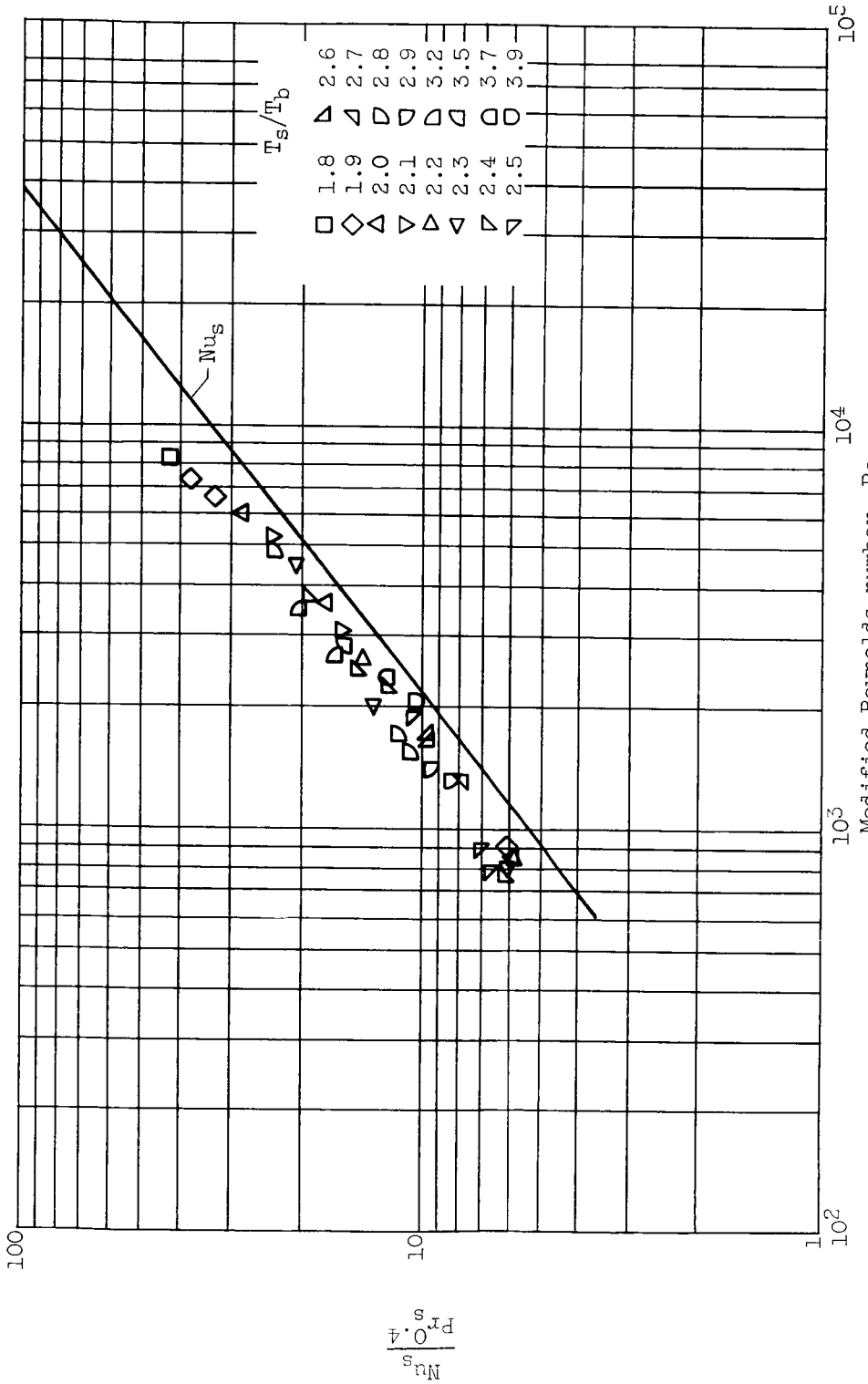

(b) Properties of helium evaluated at surface temperature T_s. Average Nusselt number $Nu_s = 0.021\ Re_s^{0.8} Pr_s^{0.4}$.

Figure 8. - Concluded. Correlation of local heat-transfer coefficients with variable heat flux. Overall length-diameter ratio, 60; bellmouth entrance.